Frontiers of Information Technology & Electronic Engineering
www.jzus.zju.edu.cn; engineering.cae.cn; www.springerlink.com
ISSN 2095-9184 (print); ISSN 2095-9230 (online)
E-mail: jzus@zju.edu.cn

Spatio-temporal correlation based incomplete time series traffic prediction for LEO satellite networks

Liang PENG†, Jie YAN†, Peng WEI, Xiaoxiang WANG†‡

Beijing University of Posts and Telecommunications, Beijing 100876, China

†E-mail: 2020010070@bupt.edu.cn; yan2023040002@bupt.edu.cn; cpwang@bupt.edu.cn

Received Dec. 26, 2023; Revision accepted Apr. 19, 2024; Crosschecked

Abstract: Accurate short-term traffic prediction is essential for improving the efficiency of data transmission in low Earth orbit (LEO) satellite networks. However, traffic values may be missing due to collector failures, transmission errors, and memory failures in complex space environments. Incomplete traffic time series prevent the efficient utilization of data, which can significantly reduce the traffic prediction accuracy. To overcome this problem, the present paper proposes a novel spatio-temporal correlation based incomplete time series traffic prediction model (ITP-ST), which consists of two phases: reconstituting the incomplete time series by missing data imputation and making traffic prediction based on the reconstructed time series. In the first phase, we propose a novel missing data imputation (IDAE-MDI) model based on the improved denoising autoencoder (DAE). Specifically, we combine DAE with the gramian angular summation field (GASF) to establish the temporal correlation between different time intervals and extract the structural patterns from the time series. Taking advantage of the unique spatio-temporal correlation of the LEO satellite network traffic, we focus on improving the missing data initialization method for DAE. In the second phase, we propose a traffic prediction (TP-CACNN) model based on a multi-channel attention mechanism convolutional neural network (CNN) by combining the spatio-temporally correlated traffic of the LEO satellite network. Finally, for achieving the ideal structure of these models, we use the multi-verse optimizer (MVO) algorithm to select the optimal combination of model parameters. Experiments on real traffic datasets show that the ITP-ST method outperforms the baseline model in terms of traffic prediction accuracy at different missing data rates, which demonstrates the effectiveness of our proposed model.

Key words: Incomplete time series; Denoising autoencoder (DAE); Spatio-temporal correlation; Traffic prediction; LEO satellite networks

https://doi.org/10.1631/FITEE.2300873 **CLC number:**

1 Introduction

Due to the high mobility of the low Earth orbit (LEO) satellites, the coverage area of each satellite varies rapidly. Factors such as population size and economic conditions in different coverage areas lead to significant differences in service traffic access to the satellites, and the dramatic changes in traffic load can easily lead to network congestion Jiang et al. (2023). Therefore, it becomes necessary to introduce traffic prediction to sense future traffic changes. However, due to collector failures, transmission errors, and memory failures in the harsh space environment, traffic values may usually be lost at unexpected moments. Such incomplete traffic time series undoubtedly creates difficulties in data analysis, which poses a significant challenge for traffic prediction in the LEO satellite networks Liu et al. (2021).

In recent decades, efforts have been devoted to solving the traffic prediction problem with incomplete time series. There are two main approaches to address the problem: the two-step approach and the synchronous approach Wang et al. (2023). In the former, the missing values in the incomplete time se-

‡ Corresponding author

ries are first filled in using a missing data imputation method. Then, predictions are made based on the reconstructed complete time series. In the latter, the imputation of missing data and the traffic prediction are synchronized.

Missing data imputation methods are the focus of research in the two-step approach, which generally include mathematical statistics and learning-based methods Baggag et al. (2021). Commonly used statistical methods include mean interpolation Mukhopadhyay and Mukherjee (2020), spline interpolation Wen-Bin et al. (2020), nearest neighbor interpolation Li et al. (2020), etc. Although these algorithms are simple and easy to implement, these methods are based on simplified smoothness and linearity assumptions, which cannot fully capture the nonlinear and uncertain variations in satellite network traffic and are only adapted to some simple linear time series.

In recent years, some learning-based methods have also been widely used for missing data imputation Miao et al. (2023), such as k-nearest neighbor (KNN), expectation-maximization (EM), generative adversarial net (GAN), denoising autoencoder (DAE), etc. For example, Marchang and Tripathi (2021) proposed a spatio-temporal k-nearest neighbor (K-NN) scheme for imputing missing data. Yoon et al. (2018) proposed a novel GAN framework for missing data imputation. Huamin et al. (2020) proposed a DAE-based model for missing data imputation and validated the model on a variety of datasets. The DAE can recover input data containing noise through unsupervised learning Nguyen et al. (2021). Missing data is a particular case of noisy inputs, making DAE an ideal model for missing data imputation Ma et al. (2023). However, the ability of DAE to extract time-dependent information from the time series is limited. Hence, a different initialization method for missing data can significantly affect the performance of missing data imputation.

After obtaining the reconstructed complete time series, some prediction algorithms need to be utilized to output the predicted values. A good traffic prediction algorithm will improve the overall performance of the incomplete time series traffic prediction. Similar to the previously mentioned missing data imputation methods, traffic prediction algorithms are also divided into two main categories: the statistical method and the deep learning method Huang et al. (2022). Statistical methods Zhao et al. (2020) such as linear regression (LR), support vector machines (SVMs), and autoregressive integrated moving average model (ARIMA). Luo et al. (2019) proposed a novel GAN framework to generate missing data in incomplete time series and then adopted SVMs to make predictions based on the reconstructed time series. Statistical-based prediction methods require the time series to be smooth. Since the satellite traffic data is extremely dynamic and highly nonlinear, these prediction methods cannot effectively analyze the future trend of satellite network traffic.

Deep learning-based prediction algorithms extract relationships directly from the data by transforming the raw data into more abstract high-level representations by using multi-layer nonlinear modules Lu et al. (2021). After ample transformations, complex and highly flexible function approximations can be realized and this helps in achieving more accurate prediction results. Ziluan and Xin (2018) proposed a generalized regression neural network (GRNN) based traffic prediction model for satellite networks. Ma et al. (2015) first introduced long short-term memory (LSTM) into traffic prediction. Some studies have also considered spatially correlated time series. For example, Ma et al. (2017) proposed a CNN-based traffic prediction model that abstracts the spatio-temporal features of traffic data into $M \times N$ matrices to extract temporal and spatial features. Ke et al. (2020) converted traffic speed and volume data into spatiotemporal multichannel matrices before training a two-stream multichannel CNN model to predict lane-level traffic speeds. They have shown that the prediction algorithms considering correlated traffic can obtain higher prediction accuracy than those that do not. However, they do not consider how different spatial time series may affect the prediction results.

Currently, most synchronization approaches are based on improved long short-term memory networks (LSTM) and gated recurrent units (GRUs), which fill in the missing data by extracting the contextual relationships of the time series while making predictions. Che Z (2018) proposed GRU-D, assuming that the missing data can be considered as a combination of the last corresponding observation and the global mean. Shen et al. (2018) proposed an end-to-end missing data imputation network with residual short paths (RIMP-LSTM), which models

a longer temporal dependency by the residual structure to produce relatively better imputation results. However, the imputation error of the missing values will be carried over to the next cycle, which leads to error accumulation.

To address the shortcomings of DAE in missing data imputation, the present paper first investigates how DAE can be improved to enhance the performance of missing data imputation. Ye et al. (2023) transformed the time series into the gramian angular summation field (GASF) images, which converts the time series into an image that describes the temporal correlation between each time point. There, by feature extraction of the GASF images, potential temporal relationships in the original time series can be mined. Deng et al. (2023) proposed an enhanced CNN model to improve CNN's temporal relation extraction capability by combining CNN with GASF. In view of this approach, the present paper combined GASF with DAE to solve the problem of DAE's poor ability to extract the temporal relationship of the time series.

The DAE often adopts the initialization method of filling in zeros for missing data. However, if the initial values are far away from the actual values, it can seriously damage the inherent temporal characteristics of the time series. Pan et al. (2023) proposed an adaptive-learned median-filled deep autoencoder (AM-DAE), which utilizes the median of the input data as the initial value for the missing values. However, this scheme does not apply to satellite network traffic, where the median value of the input data may still deviate significantly from the actual value due to the high fluctuation of satellite traffic.

Unlike ad-hoc networks and wireless sensor networks, satellite networks are highly regular and periodic. Ziluan and Xin (2018) pointed out that the correlation between the real-time traffic of different satellites at the same time is low due to the significant differences in their geographic areas. However, if a certain time lag is added, the traffic from different satellites will show a large spatio-temporal correlation. Therefore, in the present paper, to reduce the damage to the hidden temporal correlation of the time series, we use these correlated time series to improve the missing value initialization method of DAE. This spatio-temporally correlated traffic is also used as input to the traffic prediction model for improving traffic prediction accuracy.

Model parameters play a crucial role in model performance, and these parameters are usually set manually based on the experience before model learning. This practice can diminish the model's performance. Multi-verse optimizer (MVO) is a new meta-heuristic optimizer for global optimization based on the multiverse principle Appala Naidu et al. (2019). Due to its advantages such as having only a few control parameters and its robustness Kumar et al. (2018), it is widely used in optimization problems in the fieldsof engineering and finance.

The main contributions of our work are threefold:

1) We propose a novel incomplete time series traffic prediction model ITP-ST based on the spatio-temporal correlation by utilizing the unique motion regularity of the LEO satellite network. It consists of an IDAE-MDI model for missing data imputation based on an improved DAE and a TP-CACNN model for traffic prediction based on a multi-channel attention CNN.

2) In the IDAE-MDI model, we combine GASF and DAE to explicitly represent the potential relationship between each timestamp by projecting a one-dimensional time series into a two-dimensional image representation to improve the DAE's temporal correlation extraction capability. We improve the missing values initialization scheme for DAE by exploiting the unique spatio-temporal correlation of the LEO satellite networks.

3) In the TP-CACNN model, we propose a traffic prediction model based on the channel attention mechanism CNN, which utilizes spatio-temporally correlated traffic to assist in traffic prediction and considers the degree of influence of different spatio-temporally correlated traffic on the forecast.

4) We use the MVO algorithm to select the optimal combination of model parameters for the IDAE-MDI and TP-CACNN models.

The rest of the paper is organized as follows. Section 2 presents the system model and data preparation, Section 3 details the IDAE-MDI model, Section 4 details the TP-CACNN model, and Section 5 shows the evaluation results. Finally, Section 6 concludes this paper.

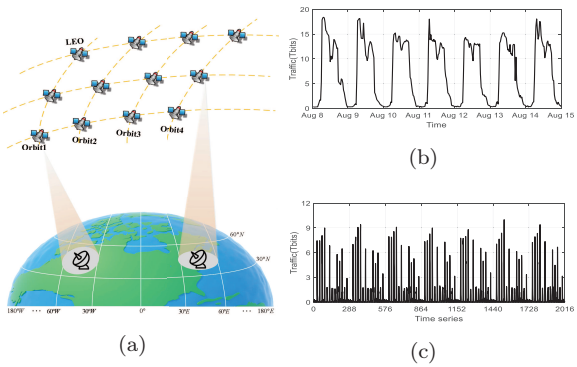

(a) (b) (c)

Fig. 1 (a) LEO satellite network traffic prediction scenarios. (b) Traffic load in the zone of $30° - 60°N$ and $90° - 120°E$. (c) Traffic time series in a satellite with a total of 2016 time sampling points.

2 Data preparation and conversion

In this subsection, we introduce the dataset and then describe converting a one-dimensional time series into a two-dimensional image using GASF.

2.1 Data preparation

Although we do not have access to the actual traffic data for the LEO satellite networks, it can be assumed that the potential traffic demand for satellite networks is proportional to the ground traffic, taking into account the bypass effect of satellite networks on the ground network Tasdemir et al. (2013). At the same time, the fundamental characteristics of ground traffic (self-similarity, long correlation, burstiness, etc.) are not changed after it passes through the terrestrial gateway into the satellite network Na et al. (2015). Therefore, the present paper will use the actual global traffic data from the 2012 Internet Census Project to translate into satellite traffic data, which collects traffic information for almost the entire global set of IPv4 addresses for nearly 6 months.

In the present paper, we construct an Iridium-like constellation consisting of 6 orbits with 11 satellites in each orbit, and each satellite having an altitude of 550 km. Each terrestrial satellite user is served by the satellite closest to it. To simplify the satellite network scenario, we uniformly divide the Earth evenly into 6×11 geographical zones and place a ground station (GS) in the center of each zone, assuming that the traffic demands of all satellite users in each zone can all be aggregated to the GS. At any given time, each GS is served by the satellite closest to it, as shown in Fig. 1a. Fig. 1b shows the traffic load from August 8, 2012, to August 15, 2012, in the zone of $30° - 60°N$ and $90° - 120°E$, which exhibits a clear characterization of the daily cycle. To calculate the traffic load on the satellite, the Iridium-like constellation and the above-mentioned traffic model were simulated using the network simulator OPNET 14.5 software. The traffic in the satellite is aggregated every 5 min, and the traffic time series for one of the satellites is shown in Fig. 1c, which exhibits a periodicity of approximately 24 h.

2.2 Time series imaging

In the present paper, traffic time series are represented as GASF feature images, which is a polar-coordinate coding algorithm that converts a one-dimensional time series into a two-dimensional feature image where each pixel shows the temporal correlation between each data point. Given a time series of n real-valued observations $\boldsymbol{x} = \{x_1, x_2, \ldots, x_n\}$, the first step is to normalize the time series to the interval $[-1, 1]$ by

$$\hat{x}_i = \frac{(x_i - x_{\max}) + (x_i - x_{\min})}{x_{\max} - x_{\min}}. \tag{1}$$

The second step converts the normalized time series into a polar coordinate representation as

$$\begin{cases} \varphi_i = \arccos(\hat{x}_i) \\ r_i = \frac{i}{N}, \end{cases} \tag{2}$$

where i is the time stamp, N is a constant parameter regulating the span of the polar coordinate system, and the angle φ_i denotes the cosine of $\hat{x}_i$. After converting to a polar coordinate system, temporal correlations over different time intervals can be identified using the trigonometric sums between each point. The GASF matrix is defined as follows Tang et al. (2023)

$$\boldsymbol{G} = [\cos(\varphi_i + \varphi_j)], \tag{3}$$

where i, j are the indexes of the elements G_{ij} in the GASF matrix. According to the trigonometric transformation, Eq. (3) is equivalent to

$$\boldsymbol{G} = \boldsymbol{x}' \cdot \hat{\boldsymbol{x}} - \sqrt{\boldsymbol{i} - \hat{\boldsymbol{x}}^2}' \cdot \sqrt{\boldsymbol{i} - \hat{\boldsymbol{x}}^2}, \tag{4}$$

where $\boldsymbol{i}$ is the unit row vector.

From the definition of GASF, it is a generalized visualization of the temporal correlation between all data points in a time series. On the one hand, the

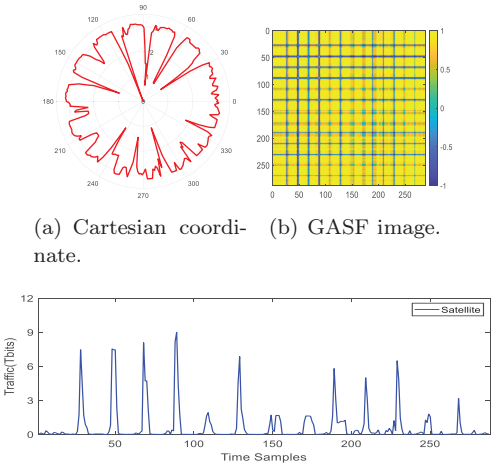

(a) Cartesian coordinate. (b) GASF image.

(c) 1 dimensional time series.

Fig. 2 Conversion of one-dimensional time series into two-dimensional GASF images.

timestamp of a data point increases as it traverses from the upper left corner to the lower right corner of the GASF matrix. On the other hand, the element G_{ij} represents the temporal correlation between x_i and x_j in the time series, and $|i-j|$ denotes the time interval between them. Moreover, the elements in the main diagonal of the GASF, $G_{ii} = \cos(2\varphi_{ii})$, which means that the raw data information is completely stored in the diagonal of the GASF. With the encoding matrix, the time series can be approximately reconstructed as GASF images, and their deep hidden features can be learned in the deep neural network. Fig. 2 shows the process of converting a one-dimensional time series of satellite traffic time series into a GASF image, where Fig. 2c is the one-dimensional time series, Fig. 2a is the transformation to the polar coordinate representation, and Fig. 2b is the GASF image.

3 Proposed IDAE-MDI model for missing data imputation

In this subsection, we introduce the basic denoising autoencoder (DAE) and how the missing value initialization method of the DAE is improved by exploiting the spatio-temporally correlated traffic of the LEO satellite network. We finally explain the training process of the IDAE-MDI model in detail.

3.1 DAE

The DAE is an unsupervised neural network that receives corrupted data as input and outputs complete data, which is widely used for image denoising and restoration Lee et al. (2022). The DAE consists of an encoder and a decoder Su et al. (2021), which are responsible for mapping the input data into a low dimensional hidden representation and reconstructing the hidden representation to the original input data, respectively. The learning process of DAE is depicted in Fig. 3. We utilize the character $\boldsymbol{x}_{actual}$ to represent the original input data, which in this paper refers to the complete traffic time series. The DAE will randomly destroy some of the data in the original input data during training to learn how to remove the noise Wang et al. (2022). We use the symbol "◯" to show the location of the data in the input data that will be destroyed. In this paper, corrupted data can be viewed as missing data. The marker vector $\boldsymbol{m}$ is introduced to indicate whether the value in the original time series $\boldsymbol{x}_{actual}$ is destroyed or not, and it is defined as

$$m_j = \begin{cases} 1 & \text{if } x_j \text{ is missing} \\ 0 & \text{otherwise.} \end{cases} \tag{5}$$

For the missing data, some initialization methods are used to fill in the missing values, and the initialized time series $\bar{\boldsymbol{x}}_{init}$ can be represented as

$$\bar{\boldsymbol{x}}_{init} = (1-\boldsymbol{m}) \odot \boldsymbol{x}_{actual} + \boldsymbol{m} \odot init(\boldsymbol{x}_{actual}), \tag{6}$$

where $init(\cdot)$ indicates the initialization method of the missing data, which is usually initialized to 0, Gaussian noise or the median, denoted by $init(\cdot) = 0$, $init(\cdot) =$ Gaussian and $init(\cdot) =$ Median, respectively.

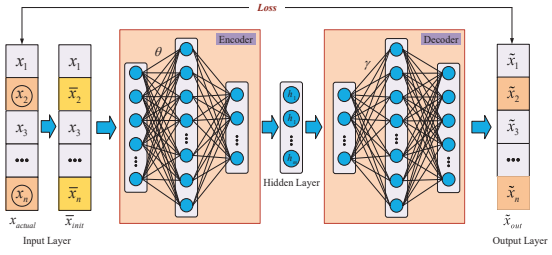

Fig. 3 Network structure of the basic DAE.

Given an initialized time series $\bar{\boldsymbol{x}}_{init}$, the encoder maps it into a hidden representation $\boldsymbol{h}$, and

then the decoder performs data reconstruction to obtain the output representation $\tilde{\boldsymbol{x}}_{out}$. The encoding and decoding functions can be defined as

$$\begin{cases} \boldsymbol{h} = \psi\left(\bar{\boldsymbol{x}}_{init}; \theta\right) \\ \tilde{\boldsymbol{x}}_{out} = \zeta\left(\boldsymbol{h}; \gamma\right), \end{cases} \tag{7}$$

where encoder $\psi(\cdot)$ and decoder $\zeta(\cdot)$ can be implemented by a fully connected neural network, a convolutional neural network, or a recurrent neural network. θ and γ are the parameters of the encoder and decoder, respectively.

The learning objective of DAE is that the output $\tilde{\boldsymbol{x}}_{out}$ is equal to the original time series $\boldsymbol{x}_{actual}$ as much as possible Tao et al. (2023). Hence, the mean squared error can be used as the loss function to learn the parameters, expressed as

$$\mathcal{L}\left(\theta, \gamma\right) = \frac{1}{N} \sum\nolimits_{n=1}^{N} ||\boldsymbol{x}_{actual} - \tilde{\boldsymbol{x}}_{out}||^2, \tag{8}$$

where $||\cdot||$ is the Frobenius Norm.

3.2 Improvements of DAE in missing data initialisation methods

Different initialization methods that are used for the missing data in the time series can significantly affect the effectiveness of data reconstruction. The time series consisting of satellite network traffic is autocorrelated Na et al. (2015). When we use the $init(\cdot) = 0$ method, if the missing value is far from 0, this will severely destroy the potential temporal relationship of the time series, and thus reduce the data reconstruction accuracy. Since the highly volatile nature of the satellite network traffic, the $init(\cdot) = Median$ method will likewise lead to a large difference between the initial value and the missing value. In other words, if the initial value is closer to the missing value, it will help DAE to extract more accurate potential temporal relationships, which will significantly improve the data reconstruction accuracy. Considering that the satellite network is a special network with regularity, the present paper will improve the initialization method $init(\cdot)$ using spatially correlated traffic.

Due to the significant differences in the geographical areas covered by different satellites at the same time, the correlation of traffic time series between satellites is low. However, due to the special motion regularity of the satellites, different satellites will have ground orbits similar to each other, and traffic time series from different satellites will show greater correlation if a certain time delay is added Ziluan and Xin (2018). For example, we illustrate this particular traffic correlation between satellites using two neighboring satellites in the same orbit as shown in Fig. 4a, and Fig. 4c shows a 24-h traffic time series for these two satellites. We define the traffic time series of satellite i as $\boldsymbol{x}^i = \left\{x_1^i, x_2^i, \ldots, x_{\mathcal{N}}^i\right\}$. Then, the Pearson correlation coefficient of the time series $\boldsymbol{x}^i$ lagging $\boldsymbol{x}^j$ with time lag l is calculated by

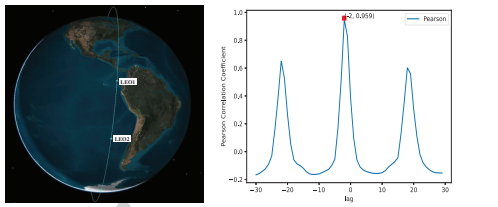

(a) (b)

(c)

Fig. 4 (a) shows two neighboring satellites in the same orbit, (c) shows the 24-h traffic time series of these two satellites, and (b) shows the correlation coefficients of those two traffic time series with different time lags.

$$\rho_{i,j}\left(l\right) = \frac{\sum_{m=1}^{\mathcal{N}} \left(x_m^i - \overline{\boldsymbol{x}^i}\right)\left(x_{m-l}^j - \overline{\boldsymbol{x}^j}\right)}{\sqrt{\sum_{m=1}^{\mathcal{N}} \left(x_m^i - \overline{\boldsymbol{x}^i}\right)^2} \sqrt{\sum_{m=1}^{\mathcal{N}} \left(x_{m-l}^j - \overline{\boldsymbol{x}^j}\right)^2}}, \tag{9}$$

where $\rho_{i,j}\left(l\right)$ denotes the degree of correlation between the current traffic of the satellite i, and the historical traffic of satellite j. There is a significant correlation between the two traffic time series when $\rho_{i,j}\left(l\right)$ is close to $+1$ or -1 Coscia and Mendez-Bermudez (2021). Fig. 4b demonstrates the Pearson correlation coefficients of these two time series at different time lags. We can see that the correlation coefficients of these two time series are significantly different with different time lags, and the correlation is the largest when satellite 1 lags satellite 2 by two sampling points.

Based on the correlation coefficients, a weight is assigned to each spatio-temporally correlated time

series, and the missing values initialized using the k most correlated time series are as follows

$$init(x_t^i) = \frac{\sum_{j=1}^{k} \Gamma_t x_t^j \rho_{i,j}(l)^{-\alpha}}{\sum_{j=1}^{k} \rho_{i,j}(l)^{-\alpha}} \tag{10}$$

where x_t^i denotes the traffic value of the i-th satellite at time t, α is a positive parameter that controls the decay rate of a satellite' weight by $\rho_{i,j}(l)^{-\alpha}$, when x_t^j is missing, Γ_t is set as 0, and otherwise, $\Gamma_t = 1$.

3.3 The MVO algorithm for model parameters optimization

The parameters such as neural network architecture, training iterations and learning rate have a significant effect on the model performance. In this paper, the MVO algorithm is used to find the optimal parameter combination to maximize the model performance. The MVO algorithm is a mathematical model intended for the optimization process by using the principle of exchange of objects between wormholes in the universe Lv et al. (2023). The MVO algorithm defines a set of universes as follows

$$U = \begin{bmatrix} u_1^1 & u_1^2 & \cdots & u_1^d \\ u_2^1 & u_2^2 & \cdots & u_2^d \\ \vdots & \vdots & \vdots & \vdots \\ u_n^1 & u_n^2 & \cdots & u_n^d \end{bmatrix} \tag{11}$$

where n is the number of universes, and each universe represents a candidate solution, d is the number of objects in the universe (i.e., the dimensionality of the solution).

After normalizing and ranking the expansion rates (fitness values) of the universe, the white hole is selected according to the roulette mechanism, and the black hole exchange dimensional information with it.

$$u_i^j = \begin{cases} u_k^j & r_1 < NI(U_i) \\ u_i^j & r_1 \geq NI(U_i) \end{cases} \tag{12}$$

where $NI(U_i)$ denotes the normalized expansion rate of the universe i, r_1 is a random number in the range of $[0, 1]$, and u_k^j denotes the j-th object of the k-th universe selected.

The wormholes are usually forwarded randomly to the universe, objects in the universe travel around the optimal universe through wormholes, and the iterative process is as follows

$$u_{ij} = \begin{cases} \begin{cases} u_0^j + T \cdot ((ub_j - lb_j) \cdot r_2 + lb_j) \\ r_3 < 0.5 \\ u_0^j - T \cdot ((ub_j - lb_j) \cdot r_2 + lb_j) \\ r_3 > 0.5 \end{cases} & r_4 > W \\ u_i^j \quad r_4 > W \end{cases} \tag{13}$$

where u_o^j is the jth variables of the best universe obtained so far, ub_j and lb_j represent the upper bound and the lower bound of jth parameter, respectively, r_2, r_3 and r_4 are the random numbers in the range of $[0, 1]$. W and T are the wormhole existence probability and traveling distance rate, respectively, and are expressed as follows

$$W = W_{\min} + l \times \left(\frac{W_{\max} - W_{\min}}{L} \right) \tag{14}$$

$$T = 1 - \frac{l^{1/p}}{L^{1/p}} \tag{15}$$

where $W_{\min}$ denotes the minimum and $W_{\max}$ denotes the maximum of the W, l is the number of current iterations, and L denotes the number of maximum repetition, and p describes the local search accuracy over the iteration.

3.4 The training process of the IDAE-MDI model

The overall framework of the IDAE-MDI model is shown in Fig. 5, and the detailed training process is shown in the following steps.

Step 1: This step is the data preparation phase, which includes the preparation of the training dataset and the finding of the k most correlated spatio-temporal traffic time series for each satellite using Eq. (9).

Step 2: This step initializes the relevant parameters of the MVO algorithm, and the population defines the IDAE-MDI model parameters, including network structure, learning factors, maximum number of training iterations, and batch size.

Step 3: This step formally enters the training session. Randomly destroy part of the data in the traffic time series $\boldsymbol{x}_{actual}$ and initialize these missing values using Eq. (10), and finally obtain $\bar{\boldsymbol{x}}_{init}$ according to Eq. (6). To improve the temporal extraction capability of the DAE, the time series $\bar{\boldsymbol{x}}_{init}$ is then converted to a two-dimensional image $\boldsymbol{G}$, i.e., GASF representation.

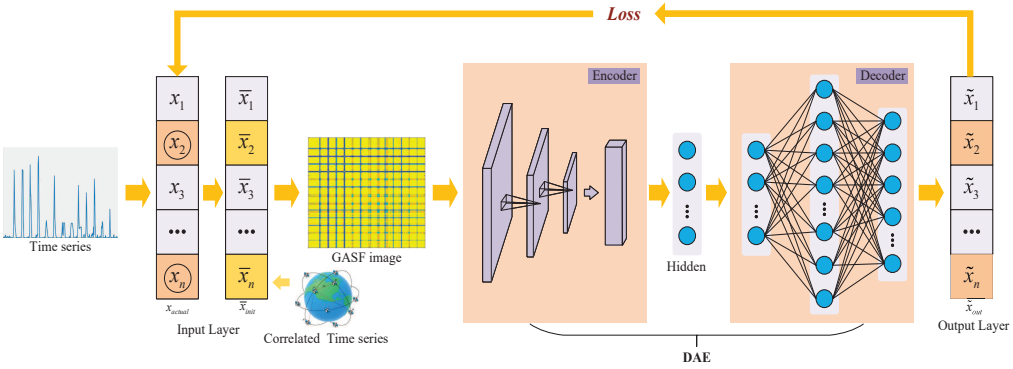

Fig. 5 The framework of the IDAE-MDI model.

Step 4: In this step, the GASF matrix $\boldsymbol{G}$ is used as the input to the DAE, and the hidden representation $\boldsymbol{h}$ is mapped by the encoder. Meanwhile, we construct the encoder with a CNN to obtain better performance in image recognition. Then the decoder outputs the reconstructed time series $\tilde{\boldsymbol{x}}_{out}$. The process is as in Eq. (7).

Step 5: This step compares the input time series $\boldsymbol{x}_{actual}$ with the output time series $\tilde{\boldsymbol{x}}_{out}$ to obtain the error function $\mathcal{L}$ in Eq. (8), and optimizes the DAE network weight parameters θ, γ using the gradient descent method.

Step 6: This step determines whether the maximum number of iterations has been reached, and if it is satisfied, then jump to Step 7; otherwise, return to Step 3.

Step 7: This step enters the next iteration of MVO, updating the population using Eq. (13), and then jumps to Step 3.

Step 8: This step determines whether the maximum iterations of the MVO algorithm have been reached, and if satisfied, ends the training, otherwise returns to Step 7.

Step 9: In this step, the trained IDAE-MDI model is used for missing data imputation for incomplete time series.

4 Proposed TP-CACNN model for traffic prediction

After imputing the missing data through the IDAE-MDI model, we predict the satellite network's traffic values for the next moment based on these reconstructed time series. In this paper, we will utilize the spatio-temporally correlated traffic mentioned above to improve traffic prediction accuracy. CNN has excellent multi-channel feature extraction capability Zhou et al. (2021), but cannot distinguish the importance of each channel. The k spatio-temporally correlated time series have different correlations with the target time series, which will have different degrees of influence on traffic prediction, so it cannot treat each correlated traffic equally. In recent years, attention-based models have been widely developed and shown their effectiveness in many fields Zhang et al. (2019a), Huang et al. (2022) uses an attention mechanism to extract the spatial relationship of traffic at different nodes, which significantly improved the accuracy of traffic prediction compared to utilizing the traffic data at only one node. Inspired by this, this paper improves the CNN by introducing a channel attention mechanism to distinguish the importance of each spatio-temporally related time series. attention mechanism. At the same time, to improve the temporal extraction ability of CNN, one-dimensional time series are still first converted into two-dimensional GASF images. The overall framework is shown in Fig. 6, and the steps are given as follows.

Step 1: This step is the data processing phase, where the target time series and the k most relevant spatio-temporal time series are transformed into a two-dimensional GASF feature image. When the length of the time series is N, we can obtain a feature map $\boldsymbol{x} \in \mathbb{R}^{K\times N\times N}$. Specifically, we can denote $\boldsymbol{x} = \left[\boldsymbol{x}^1, \boldsymbol{x}^2, \ldots, \boldsymbol{x}^K\right]$, where $\boldsymbol{x}^c \in \mathbb{R}^{N\times N}$ represents the channel c of $\boldsymbol{x}$.

Step 2: This step gives the attention weights for each channel and generates the refined feature map with attention weights. Since the k spatio-

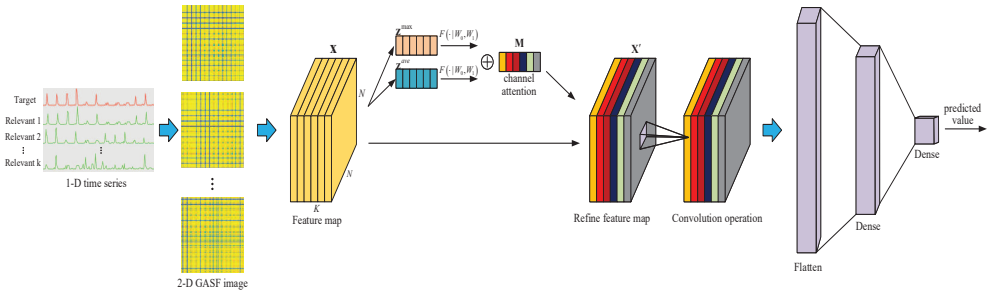

Fig. 6 Principle of TP-CACNN model.

temporally correlated time series have different correlations with the target time series, they have different degrees of influence on traffic prediction. Therefore, the TP-CACNN model first adds a channel attention mechanism to adaptively assign channel weights to distinguish the importance of each spatio-temporally correlated time series. We squeeze the global feature map $\boldsymbol{x}$ using global average pooling and maximum pooling to generate two channel-level statistics: $\boldsymbol{z}^{ave}$ and $\boldsymbol{z}^{max}$, respectively. Formally, the statistic $\boldsymbol{z}^{ave}$ and $\boldsymbol{z}^{max}$ are erased by shrinking $\boldsymbol{x}$ through spatio-temporal dimensions $N \times N$, where the c-th elements of $\boldsymbol{z}^{ave}$ and $\boldsymbol{z}^{max}$ are calculated by

$$z_c^{ave} = \frac{1}{N^2} \sum_{i=1}^{N} \sum_{j=1}^{N} x^c(i,j), \tag{16}$$

$$z_c^{max} = \max(x^c(i,j)), \tag{17}$$

where z_c^{ave} and z_c^{max} can represent the information of channel c, respectively. Then z_c^{ave} and z_c^{max} are forwarded to a shared network to produce our channel attention map. The shared network is composed of a multi-layer perceptron (MLP) with one hidden layer and has the same number of neurons in the input and output layers. After the shared network is applied to each descriptor, we merge the output feature vectors using element-wise summation. In short, the channel attention $\boldsymbol{M} \in \mathbb{R}^{K \times 1 \times 1}$ is computed as

$$\boldsymbol{M} = \sigma\left(\boldsymbol{W}_1\left(\boldsymbol{W}_0\left(\boldsymbol{z}^{ave}\right)\right) + \boldsymbol{W}_1\left(\boldsymbol{W}_0\left(\boldsymbol{z}^{\max}\right)\right)\right), \tag{18}$$

where σ denotes the sigmoid function, $\boldsymbol{W}_0$ and $\boldsymbol{W}_1$ are neural network weights. Finally, the refined feature map $\boldsymbol{x}'$ after channel attention processing is obtained as

$$\boldsymbol{x}' = \boldsymbol{x} \otimes \boldsymbol{M}, \tag{19}$$

where $\otimes$ refers to channel-wise multiplication between the feature map $\boldsymbol{x}$ and channel attention $\boldsymbol{M}$.

Step 3: This step initializes the relevant parameters of the MVO algorithm, and the population defines the TP-CACNN model parameters, including network structure, learning factors, maximum number of training iterations, and batch size.

Step 4: In this step, the TP-CACNN model enters the training phase. The refined feature map $\boldsymbol{x}'$ is input to the CNN, and each channel performs a convolution operation with the convolution kernel. Then, the computed results of each channel are summed up by channel and inputted to the fully connected layer to get the predicted value. Finally, the predicted values are compared with the true values, and the training parameters are optimized using the gradient descent.

Step 5: This step determines whether the maximum number of iterations has been reached, and if it is satisfied, then jump to Step 6; otherwise, return to Step 4.

Step 6: This step enters the next iteration of MVO, updating the population using Eq. (13), and then jumps to Step 4.

Step 7: This step determines whether the maximum iterations of the MVO algorithm have been reached, and if satisfied, ends the training, otherwise returns to Step 6.

Step 8: In this step, the trained TP-CACNN model is used for traffic prediction.

5 Simulation results

5.1 Experiment design

We evaluate the proposed model based on the previously described dataset obtained from the 2012 Internet Census Project, where the first 80% as the training set and the last 20% as the test set. To validate the performance of the proposed model with

different data missing rates, we randomly masked some of the data in the dataset with data missing rates of 10%, 20%, 30%, 40%, and 50%. Meanwhile, to evaluate the proposed model performance more comprehensively and avoid possible inaccuracies due to data and calculation restrictions, we conducted experiments on a total of three satellites.

The root mean square error (RMSE) is used as our evaluation metric to compare the accuracy of missing value imputation of different methods, expressed as follows

$$RMSE = \sqrt{\frac{1}{\mathcal{N}} \sum_{i=1}^{\mathcal{N}} (x_{actual} - \tilde{x}_{out})^2}, \tag{20}$$

where $\mathcal{N}$ denotes the number of time samples, and $\tilde{x}$ and x_{actual} represent the imputation of missing values and real data, respectively. The smaller the RMSE value, the better the performance of the model.

5.2 Complexity analysis

In this subsection, the time complexity of the proposed ITP-ST model is analyzed, which is jointly determined by the IDAE-MDI and TP-CACNN models. The IDAE-MDI model mainly contains a CNN network $\psi(\theta)$ and a FC network $\zeta(\gamma)$. Suppose $\psi(\theta)$ contains $\mathcal{L}_\psi$ convolutional layers, and $\zeta(\gamma)$ contains $\mathcal{L}_\zeta$ fully connected layers. The time complexity of the IDAE-MDI model is expressed as

$$O\left(\sum_{l=0}^{L_\psi} {N_l}^2 {K_l}^2 + \sum_{l=0}^{L_{\zeta-1}} \zeta_l \zeta_{l+1}\right) \tag{21}$$

where N_0 denotes the length of the time series, K denotes the size of the convolutional kernel, and ζ_l denotes the number of neurons in the l-th layer. The TP-CACNN model is a multi-channel CNN network $\varsigma(\omega)$ with an attention mechanism, andthe time complexity of the TP-CACNN model can be expressed as

$$O\left(N_0^2 \cdot C + \sum_{l=0}^{L_\varsigma} {N_l}^2 \cdot {K_l}^2 \cdot C\right) \tag{22}$$

where C_l defines the number of input channels in the l-th layer.

5.3 Experimental results and analysis

1) Model parameters optimization results: Figs. 7a-b illustrate the search process for the optimal parameters of IDAE-MDI and TP-CACNN models, respectively. The optimal model parameters are shown in Table 1.

Table 1 Optimal model parameters

Model	Parameters	Values
IDAE-MDI	Encoder	$64 * 64$
	Hidden layer h	28
	Dncoder	$28 * 171 * 64$
	Learning factors l	3.079e-5
	Batch size *batch*	32
	training iterations	116
TP-CACNN	Input size	$64 * 64$
	Fully connected layer	$126 * 54 * 1$
	Learning factors l	1.62e-5
	Batch size *batch*	32
	training iterations	98

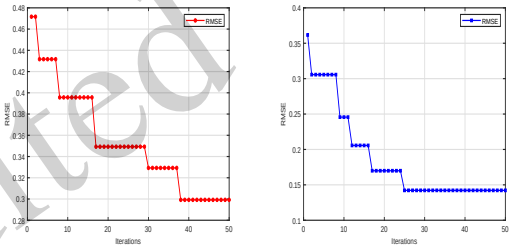

(a) IDAE-MDI model. (b) TP-CACNN model.

Fig. 7 The search process for the optimal parameters of thr IDAE-MDI and TP-CACNN models.

2) Ablation experiments on the IDAE-MDI model: To verify the extent to which the improvement of DAE affects the imputation of missing data, we compared the performance of the IDAE-MDI model and its variants through ablation experiments. The different variants of the IDAE-MDI model are as follows.

- **DAE-1D-Zero**: This is the base DAE, where the input is a one-dimensional time series, and the missing data are initialized to zero.
- **DAE-1D-Median**: The input to the DAE is a one-dimensional time series, and the missing data initialized to the median value of the input.
- **DAE-1D-Related**: The input to the DAE is a one-dimensional time series, and the missing data are initialized using the missing data initialization method proposed in this paper.
- **DAE-2D-Zero**: The input to the DAE is a two-dimensional time series that has been transformed by GASF, and the missing data are ini-

tialized to zero.

- **DAE-2D-Median**: The input to the DAE is a two-dimensional time series, and the missing data initialized to the median of the inputs.
- **IDAE-MDI**: This is the model proposed in this paper, where the input is a GASF-transformed two-dimensional time series, and the missing data are initialized using spatio-temporally correlated time series.

To evaluate the advantages of the IDAE-DMI model in terms of computational efficiency and accuracy, we conducted experiments on these two aspects separately. Fig. 8 illustrates the comparison of the convergence times of the IDAE-MDI model and its variants at different missing data rates, and we can see that the IDAE-MDI model has a faster computational efficiency. We visualized the training process with a missing rate of 10%, as shown in Fig. 9, where each point indicates the RMSE value of the test set during the training process.

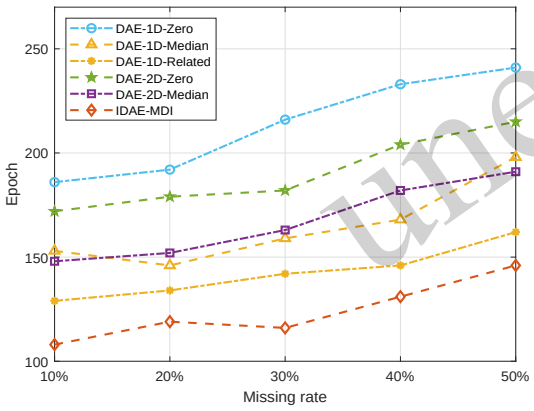

Fig. 8 Comparison of convergence times of the IDAE-MDI model and its variants at different missing data rates.

Table 2 shows in detail the RMSE of the IDAE-MDI model and its variants for missing data imputation for a total of three satellites. We averaged the RMSE values of the three satellites, as shown in Fig. 10. It can be seen that the IDAE-MDI model outperforms its variants in terms of accuracy of missing data imputation at different missing rates. When DAE uses the same missing data initialization method, transforming one-dimensional time series into GASF matrices has better accuracy in missing data imputation, e.g., DAE-1D-Zero and DAE-2D-Zero. When DAE uses the same input methods, such

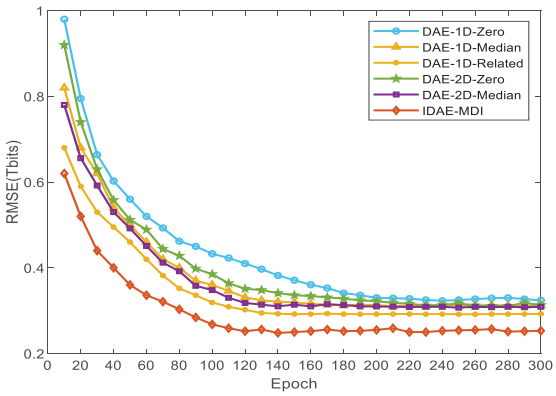

Fig. 9 RMSE comparison of IDAE-MDI models and their variants during training at 10% missing data rate.

as DAE-2D-Zero, DAE-2D-Median, and IDAE-MDI, it is better to use the initialization of the correlated traffic rather than the median and zero. Moreover, DAE-1D-Related has better missing data imputation accuracy than DAE-2D-Zero and DAE-2D-Median, indicating that the initialization method using correlated traffic has a more significant impact compared to transforming one-dimensional time series into GASF matrices.

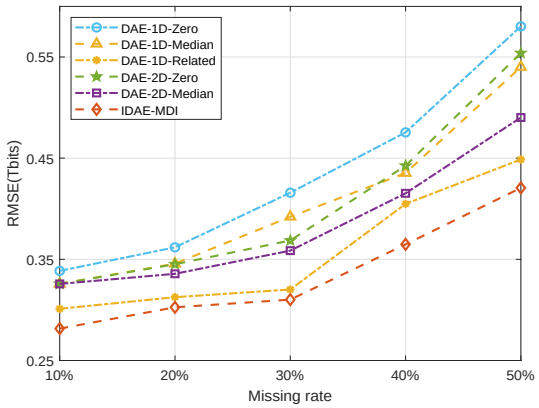

Fig. 10 Comparison of the RMSE of the IDAE-MDI model and its variants at different missing data rates.

3) Comparison of the performance of the IDAE-MDI model with the baseline model for missing data imputation: To evaluate the performance of the IDAE-MDI model, we compare it with the following baseline methods commonly used for missing data imputation.

- **Spline** Wen-Bin et al. (2020): The spline interpolation is used for the imputation of the missing data.

Table 2 Comparison on RMSE of different methods

Models	Satellite 1					Satellite 2					Satellite 3				
	10%	20%	30%	40%	50%	10%	20%	30%	40%	50%	10%	20%	30%	40%	50%
DAE-1D-Zero	0.3262	0.3529	0.408	0.4826	0.578	0.34	0.3618	0.427	0.4728	0.5903	0.3494	0.3708	0.4125	0.471	0.5724
DAE-1D-Median	0.338	0.3386	0.3987	0.4287	0.536	0.319	0.365	0.387	0.448	0.5493	0.32	0.3914	0.3903	0.429	0.535
DAE-1D-Related	0.309	0.318	0.3302	0.406	0.45	0.2971	0.3219	0.328	0.396	0.442	0.2972	0.2978	0.3022	0.4124	0.4541
DAE-2D-Zero	0.3279	0.344	0.3594	0.463	0.5603	0.3183	0.325	0.372	0.4322	0.5411	0.3308	0.338	0.374	0.4225	0.56
DAE-2D-Median	0.32	0.3325	0.3603	0.425	0.502	0.337	0.327	0.352	0.408	0.4953	0.3208	0.347	0.363	0.4127	0.473
Spine	0.3905	0.4787	0.5836	0.756	0.9856	0.4203	0.4669	0.6035	0.689	1.109	0.4148	0.4698	0.5704	0.7314	1.146
KNN-ST	0.319	0.358	0.4398	0.486	0.653	0.3287	0.3627	0.426	0.503	0.605	0.3127	0.3763	0.4148	0.486	0.591
GRU-D	0.3104	0.336	0.384	0.44	0.567	0.298	0.3263	0.362	0.4896	0.603	0.319	0.3147	0.3777	0.458	0.6269
IDAE-MDI(WM)	0.2939	0.2989	0.327	0.335	0.398	0.2939	0.3087	0.3094	0.3603	0.402	0.2568	0.307	0.304	0.3991	0.4617
IDAE-MDI	**0.2403**	**0.2668**	**0.2826**	**0.3199**	**0.3824**	**0.2309**	**0.2693**	**0.2932**	**0.3201**	**0.3787**	**0.2474**	**0.0.2516**	**0.2947**	**0.3344**	**0.379**

- **KNN** Marchang and Tripathi (2021): The missing data are imputed using KNN.
- **GRU-D** Che Z (2018): Learning the temporal properties of a time series to compute missing data using an improved GRU.
- **IDAE-MDI(WM)**: IDAE-MDI model without parameter optimization by the MVO algorithm.

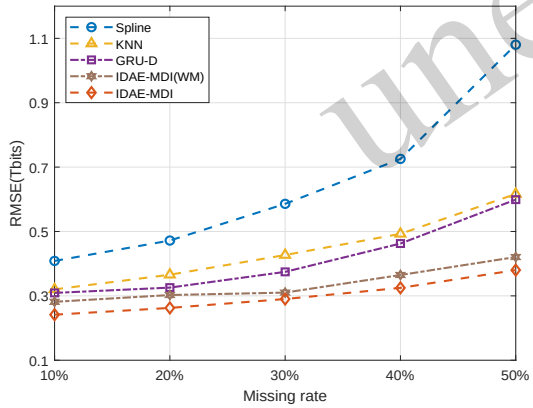

Fig. 11 Comparison of the RMSE of the IDAE-MDI model and the baseline models at different missing data rates.

Fig. 11 shows the comparison of RMSE between the IDAE-MDI model and the baseline model for imputing missing data at different missing rates, and it can be seen that the IDAE-MDI model outperforms the baseline model in the imputation of missing data at different missing rates. The RMSE of different models increases with the increase of missing data rate, but the RMSE of the IDAE-MDI model grows more slowly. The spline interpolation method performs well at low missing data rate, but the accuracy decreases rapidly as the missing rate increases. As the missing rate increases, the GRU-D model accumulates too much error, which leads to a rapid decrease in the accuracy of missing data imputation.

4) Comparison of the performance of the TP-CACNN model with the baseline models for time series traffic prediction: To validate the performance of the TP-CACNN model, we compare the TP-CACNN model with the following baseline models based on the complete time series.

- **SVM**: SVM, a traditional statistics-based machine learning algorithm.
- **LSTM** Ma et al. (2015):LSTM networks, a recurrent neural network commonly used for time series prediction, which can extract temporal relationships in time series.
- **CNN-MC** Ke et al. (2020): Multiple spatio-temporally relevant traffic are used as CNN inputs, but the degree of influence of different spatio-temporal traffic on the traffic prediction is not considered.
- **TP-CACNN(WM)**: TP-CACNN model without parameter optimization by the MVO algorithm.

Table 3 shows in detail the RMSEs of the TP-CACNN model and its baseline model for time series traffic forecasts for a total of three LEO satellites. We can see that the traffic prediction accuracy is higher due to the consideration of spatio-temporally correlated traffic by the CNN-MC model and the TP-CACNN model. TP-CACNN has a lower RMSE than CNN-MC, which proves the effectiveness of the introduced multi-channel attention mechanism. Fig.

Table 4 Comparison on RMSE of different models

Models	Satellite 1					Satellite 2					Satellite 3				
	10%	20%	30%	40%	50%	10%	20%	30%	40%	50%	10%	20%	30%	40%	50%
Spine-GRU	0.4258	0.4425	0.482	0.5063	0.6049	0.3914	0.436	0.5019	0.546	0.582	0.4084	0.417	0.4736	0.5841	0.6207
GAN-SVM	0.3853	0.3659	0.4426	0.4588	0.578	0.3524	0.3761	0.4372	0.473	0.5533	0.3679	0.4035	0.4277	0.4924	0.5263
GRU-D	0.3566	0.375	0.4308	0.4431	0.4589	0.3328	0.3692	0.418	0.462	0.4819	0.3476	0.35125	0.3872	0.4226	0.4949
RIMP-LSTM	0.3106	0.3363	0.3522	0.4027	0.4339	0.3028	0.3004	0.3666	0.4055	0.429	0.3036	0.3403	0.3569	0.3775	0.3975
DRMI-GRU	0.3025	0.3106	0.3392	0.3698	0.4059	0.2806	0.3261	0.3402	0.3709	0.4022	0.2858	0.3211	0.341	0.3837	0.3936
ITP-ST	**0.2356**	**0.2783**	**0.2599**	**0.2907**	**0.3162**	**0.2501**	**0.269**	**0.308**	**0.3002**	**0.3144**	**0.2689**	**0.2604**	**0.2725**	**0.2935**	**0.3011**

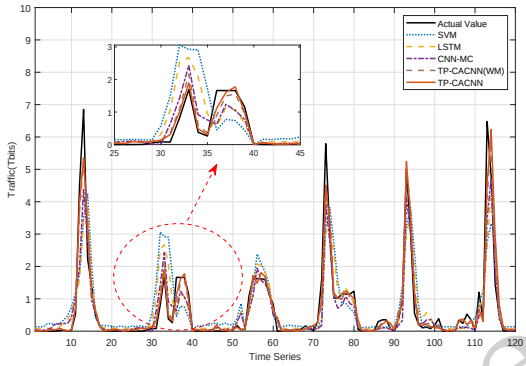

Fig. 12 Comparison curves of the true and predicted values for four different models.

Table 3 RMSE metrics for different models for each satellite.

Models	Satellite		
	Satellite 1	Satellite 2	Satellite 3
SVM	0.2814	0.2604	0.2908
LSTM	0.2305	0.2114	0.2349
CNN-MC	0.2121	0.1935	0.2197
TP-CACNN(WM)	0.1682	0.1802	0.1814
TP-CACNN	**0.1506**	**0.1492**	**0.1449**

12 shows the comparison curves between the true and predicted values of four different models for one of the satellites.

5) Comparison of the performance of the ITP-ST model with the baseline model for incomplete time series traffic prediction: To validate the overall performance of the ITP-ST model, we compare the ITP-ST model with the following baseline model.

- **Spline-GRU**: The spline interpolation is used for the imputation of the missing data, and utilize GRU for traffic prediction.
- **GAN-SVM** Luo et al. (2019): GAN is used to generate missing data in incomplete time series and then SVM is utilized to predict based on the reconstructed time series.
- **GRU-D** Che Z (2018): A synchronization method that implements missing data imputation and traffic prediction by means of an improved GRU to extract temporal attributes of incomplete time series.
- **RIMP-LSTM** Shen et al. (2018): A synchronization method that fuses the LSTM structure with residual shortcut connection and takes into account the previously observed values and the overall observed in a sample set.
- **DRMI-GRU** Zhang et al. (2019b):Fuse the GRU structure with residual shortcut connection and takes into account the previously observed values and the overall observed in a sample set.

Table 3 shows the RMSE of the ITP-ST model and its baseline model for incomplete time series traffic prediction at different data missing rates for a total of three satellites. We averaged the RMSE values of the three satellites, as shown in Fig. 13. We can see that the ITP-ST model outperforms the baseline model under different missing rates. When

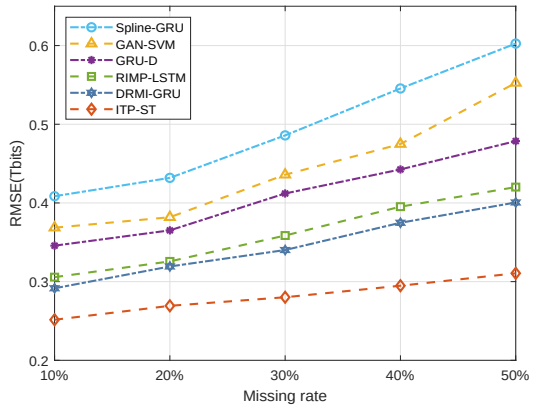

Fig. 13 Comparison of the RMSE of the ITP-ST model and the baseline models at different missing data rates.

the missing rate is small (e.g., 10%), the difference in performance between the different models is not significant. This is mainly because different models perform well in missing data imputation at a low missing rate. The RMSE of each model grows with the increase of missing rate, but the RMSE of the ITP-ST model grows slowly. The traffic prediction accuracy in the Spline-GRU model decreases rapidly with the increase of missing rate. In the GRU-D and RIMP-LSTM models, it does not lead to significant performance degradation as the missing rate increases due to the strong temporal extraction capability of GRU and LSTM.

6 Conclusions

This paper proposed a novel spatio-temporal correlation-based incomplete time series traffic prediction model for LEO satellite networks, i.e., ITP-ST. It consists of an IDAE-MDI model for missing data imputation and a TP-CACNN model for traffic prediction. The IDAE-MDI model is based on an improved DAE. Firstly, we combined GASF and DAE to explicitly represent the potential relationship between each timestamp by projecting the one-dimensional time series into a two-dimensional image representation. Secondly, we took advantage of the unique spatio-temporal correlation of the LEO satellite network to improve the missing value initialization scheme of DAE. After obtaining the reconstructed time series, we performed traffic prediction using the proposed TP-CACNN, which takes into account the degree of influence of different spatio-temporally correlated traffic on traffic prediction. Finally, to achieve the ideal structure of these models, we used the MVO algorithm to select the optimal combination of model parameters. Experiments on real traffic datasets show that the ITP-ST method outperforms the baseline model in terms of traffic prediction accuracy at different missing data rates, which demonstrates the effectiveness of our proposed model.

Contributors

Liang PENG designed the research. Jie YAN and Peng WEI processed the data. Liang PENG drafted the manuscript. Jie YAN helped organize the manuscript. Xiaoxiang WANG revised and finalized the paper.

Conflict of interest

All the authors declare that they have no conflict of interest.

Data availability

Due to the nature of this research, participants of this study did not agree for their data to be shared publicly, so supporting data is not available.

References

Appala Naidu T, Raj Arya S, Maurya R, 2019. Dynamic voltage restorer with quasi-newton filter-based control algorithm and optimized values of pi regulator gains. *IEEE J Emerg Sel Top Power Electron*, 7(4):2476-2485. https://doi.org/10.1109/JESTPE.2018.2890415

Baggag A, Abbar S, Sharma A, et al., 2021. Learning spatiotemporal latent factors of traffic via regularized tensor factorization: Imputing missing values and forecasting. *IEEE Trans Knowl Data Eng*, 33(6):2573-2587. https://doi.org/10.1109/TKDE.2019.2954868

Che Z Purushotham S CKSDLY, 2018. Recurrent Neural Networks for Multivariate Time Series with Missing Values. *Sci Rep*, 8(18):6085. https://doi.org/10.1038/s41598-018-24271-9

Coscia M, Mendez-Bermudez A, 2021. Pearson correlations on complex networks. *J Complex Netw*, 9(6):1-14. https://doi.org/10.1093/comnet/cnab036

Deng B, Xu T, Yan M, 2023. UWB NLOS identification and mitigation based on gramian angular field and parallel deep learning model. *IEEE Sens J*, :1-1. https://doi.org/10.1109/JSEN.2023.3323564

Huamin T, Qiuqun D, Shanzhu X, 2020. Reconstruction of time series with missing value using 2D representation-based denoising autoencoder. *J Syst Eng Electoron*, 31(6):1087-1096. https://doi.org/10.23919/JSEE.2020.000081

Huang J, Luo K, Cao L, et al., 2022. Learning multiaspect traffic couplings by multirelational graph attention networks for traffic prediction. *IEEE Trans Intell Transp*

Syst, 23(11):20681-20695.
https://doi.org/10.1109/TITS.2022.3173689

Jiang B, Yan Y, You L, et al., Apr 2023. Robust secure transmission for satellite communications. *IEEE Trans Aerosp Electron Syst*, 59(2):1598-1612.
https://doi.org/10.1109/TAES.2022.3203027

Ke R, Li W, Cui Z, et al., 2020. Two-stream multi-channel convolutional neural network for multi-lane traffic speed prediction considering traffic volume impact. *Transp Res Record*, 2674(4):459-470.
https://doi.org/10.1177/0361198120911052

Kumar P, Garg S, Singh A, et al., 2018. Mvo-based 2-d path planning scheme for providing quality of service in uav environment. *IEEE Internet Things J*, 5(3):1698-1707.
https://doi.org/10.1109/JIOT.2018.2796243

Lee WK, Seo HJ, Seo SC, et al., 2022. Efficient implementation of AES-CTR and AES-ECB on GPUs with applications for high-speed FrodoKEM and exhaustive key search. *IEEE Trans Circuits Syst II-Express Briefs*, 69(6):2962-2966.
https://doi.org/10.1109/TCSII.2022.3164089

Li F, Shang C, Li Y, et al., 2020. Interpolation with just two nearest neighboring weighted fuzzy rules. *IEEE Trans Fuzzy Syst*, 28(9):2255-2262.
https://doi.org/10.1109/TFUZZ.2019.2928496

Liu W, Ren C, Xu Y, 2021. PV Generation Forecasting With Missing Input Data: A Super-Resolution Perception Approach. *IEEE Trans Sustain Energy*, 12(2):1493-1496.
https://doi.org/10.1109/TSTE.2020.3029731

Lu BL, Liu ZH, Wei HL, et al., 2021. A deep adversarial learning prognostics model for remaining useful life prediction of rolling bearing. *IEEE Trans Artif Intell*, 2(4):329-340.
https://doi.org/10.1109/TAI.2021.3097311

Luo Y, Zhang Y, Cai X, et al., 2019. EÂšGAN: End-to-end generative adversarial network for multivariate time series imputation. Proc 28th Int Joint Conf on Artificial Intelligence, p.3094-3100.

Lv Z, Peng L, Cao Y, et al., 2023. Weak fault feature extraction method of rolling bearings based on mvo-momeda under strong noise interference. *IEEE Sens J*, 23(14):15732-15740.
https://doi.org/10.1109/JSEN.2023.3277516

Ma Q, Lee W, Fu T, et al., 2023. MIDIA: exploring denoising autoencoders for missing data imputation. *Data Min Knowl Disc*, 34:1859-1897.
https://doi.org/10.1007/s10618-020-00706-8

Ma X, Tao Z, Wang Y, et al., 2015. Long short-term memory neural network for traffic speed prediction using remote microwave sensor data. *Transp Res Part C Emerg Technol*, 54:187-197.
https://doi.org/10.1016/j.trc.2015.03.014

Ma X, Dai Z, He Z, et al., 2017. Learning traffic as images: A deep convolutional neural network for large-scale transportation network speed prediction. *Sensors*, 17(4):818.
https://doi.org/10.3390/s17040818

Marchang N, Tripathi R, 2021. KNN-ST: Exploiting spatio-temporal correlation for missing data inference in environmental crowd sensing. *IEEE Sens J*, 21(3):3429-3436.
https://doi.org/10.1109/JSEN.2020.3024976

Miao X, Wu Y, Chen L, et al., 2023. An experimental survey of missing data imputation algorithms. *IEEE Trans Knowl Data Eng*, 35(7):6630-6650.
https://doi.org/10.1109/TKDE.2022.3186498

Mukhopadhyay S, Mukherjee A, 2020. ImdLMS: An imputation based LMS algorithm for linear system identification with missing input data. *IEEE Trans Signal Process*, 68:2370-2385.
https://doi.org/10.1109/TSP.2020.2983162

Na Z, Liu Y, Cui Y, et al., 2015. Research on aggregation and propagation of self-similar traffic in satellite network. *Int J Hybrid Inf Technol*, 8:325-338.
https://doi.org/10.14257/ijhit.2015.8.1.29

Nguyen HD, Vu TL, Slotine JJ, et al., 2021. Contraction analysis of nonlinear DAE systems. *IEEE Trans Autom Control*, 66(1):429-436.
https://doi.org/10.1109/TAC.2020.2981348

Pan Z, Wang Y, Wang K, et al., 2023. Imputation of missing values in time series using an adaptive-learned median-filled deep autoencoder. *IEEE T Cybern*, 53(2):695-706.
https://doi.org/10.1109/TCYB.2022.3167995

Shen L, Ma Q, Li S, 2018. End-to-End Time Series Imputation via Residual Short Paths. Proc 10th Asian Conf on Machine Learning Research, p.248-263.

Su T, Liu Y, Zhao J, et al., 2021. Probabilistic stacked denoising autoencoder for power system transient stability prediction with wind farms. *IEEE Trans Power Syst*, 36(4):3786-3789.
https://doi.org/10.1109/TPWRS.2020.3043620

Tang D, Wang S, Liu B, et al., 2023. GASF-IPP: Detection and mitigation of LDoS attack in SDN. *IEEE Trans Serv Comput*, 16(5):3373-3384.
https://doi.org/10.1109/TSC.2023.3266757

Tao X, Liu Z, Zhao F, et al., 2023. An SSA-LC-DAE method for extracting network security elements. *IEEE Trans Netw Sci Eng*, 10(2):1175-1185.
https://doi.org/10.1109/TNSE.2023.3233986

Tasdemir Y, Kolay E, Kayabali K, 2013. Comparison of three artificial neural network approaches for estimating of slake durability index. *Environmental Earth Sciences*, 68:23-31.
https://doi.org/10.1007/s12665-012-1702-3

Wang A, Ye Y, Song X, et al., 2023. Traffic prediction with missing data: A multi-task learning approach. *IEEE Trans Intell Transp Syst*, 24(4):4189-4202.
https://doi.org/10.1109/TITS.2022.3233890

Wang HY, Zhao JP, Su YS, et al., 2022. scCDG: A method based on DAE and GCN for scRNA-Seq data analysis. *IEEE-ACM Trans Comput Biol Bioinform*, 19(6):3685-3694.
https://doi.org/10.1109/TCBB.2021.3126641

Wen-Bin Y, Yong-Hong D, Yue Y, Mar 2020. Static explosion field reconstruction based on the improved biharmonic spline interpolation. *IEEE Sens J*, 20(13):7235-7240.
https://doi.org/10.1109/JSEN.2020.2978502

Ye L, Hu S, Yan T, et al., 2023. GAF representation of millimeter wave drone RCS and drone classification method based on deep fusion network using resnet. *IEEE Trans Aerosp Electron Syst*, 59(1):336-346.
https://doi.org/10.1109/TAES.2022.3182303

Yoon J, Jordon J, Schaar M, 2018. Gain: Missing data imputation using generative adversarial nets. Proc 35th Int conf on machine learning, p.5689-5698.

Zhang C, Yu JJQ, Liu Y, 2019a. Spatial-temporal graph attention networks: A deep learning approach for traffic forecasting. *IEEE Access*, 7:166246-166256. https://doi.org/10.1109/ACCESS.2019.2953888

Zhang J, Mu X, Fang J, et al., 2019b. Time series imputation via integration of revealed information based on the residual shortcut connection. *IEEE Access*, 7:102397-102405. https://doi.org/10.1109/ACCESS.2019.2928641

Zhao L, Song Y, Zhang C, et al., 2020. T-GCN: A temporal graph convolutional network for traffic prediction. *IEEE Trans Intell Transp Syst*, 21(9):3848-3858. https://doi.org/10.1109/TITS.2019.2935152

Zhou X, Shi J, Gong K, et al., 2021. A novel quench detection method based on CNN-LSTM model. *IEEE Trans Appl Supercond*, 31(5):1-5. https://doi.org/10.1109/TASC.2021.3070735

Ziluan L, Xin L, Fed 2018. Short-term traffic forecasting based on principal component analysis and a generalized regression neural network for satellite networks. *J China Univ Posts and Telecommun*, 25:15-28. https://doi.org/10.19682/j.cnki.1005-8885.2018.0002